Opto-Electronic Science

ISSN 2097-0382 CN 51-1800/O4

Vectorial spin-orbital Hall effect of light upon tight focusing and its experimental observation in azopolymer films

Alexey Porfirev, Svetlana Khonina, Andrey Ustinov, Nikolay Ivliev and Ilya Golub

Citation: Porfirev A, Khonina S, Ustinov A, Ivliev N, Golub I. Vectorial spin-orbital Hall effect of light upon tight focusing and its experimental observation in azopolymer films. *Opto-Electron Sci* **2**, 230014 (2023).

https://doi.org/10.29026/oes.2023.230014

Received: 7 June 2023; Accepted: 20 July 2023; Published online: 27 September 2023

Opto-Electronic Science

Article

July 2023, Vol. 2, No. 7

DOI: 10.29026/oes.2023.230014

Vectorial spin-orbital Hall effect of light upon tight focusing and its experimental observation in azopolymer films

Alexey Porfirev[1]*, Svetlana Khonina[1], Andrey Ustinov[1], Nikolay Ivliev[1] and Ilya Golub[2]

Hall effect of light is a result of symmetry breaking in spin and/or orbital angular momentum (OAM) possessing optical system and is caused by e.g. refractive index gradient/interface between media or focusing of a spatially asymmetrical beam, similar to the electric field breaking the symmetry in spin Hall effect for electrons. The angular momentum (AM) conservation law in the ensuing asymmetric system dictates redistribution of spin and orbital angular momentum, and is manifested in spin-orbit, orbit-orbit, and orbit-spin conversions and reorganization, i.e. spin-orbit and orbit-orbit interaction. This AM restructuring in turn requires shifts of the barycenter of the electric field of light. In the present study we show, both analytically and by numerical simulation, how different electric field components are displaced upon tight focusing of an asymmetric light beam having OAM and spin. The relation between field components shifts and the AM components shifts/redistribution is presented too. Moreover, we experimentally demonstrate, for the first time, to the best of our knowledge, the spin-orbit Hall effect of light upon tight focusing in free space. This is achieved using azopolymers as a media detecting longitudinal or *z* component of the electrical field of light. These findings elucidate the Hall effect of light and may broaden the spectrum of its applications.

Keywords: spin-orbital Hall effect of light; symmetry breaking; spin-orbit interaction; azopolymers; optical vortex; polarization

Porfirev A, Khonina S, Ustinov A, Ivliev N, Golub I. Vectorial spin-orbital Hall effect of light upon tight focusing and its experimental observation in azopolymer films. *Opto-Electron Sci* **2**, 230014 (2023).

Introduction

Removal/breaking of symmetry is a widespread occurrence in nature resulting in useful and unique phenomena such as ferromagnetism[1], weak nuclear force[2], prevalence of certain handedness in living matter[3,4], topological phase transitions in spin-orbit optics[5], etc. One of the most prominent effects due to breaking the symmetry of a light field is spin-orbital Hall effect of light[6–12]. Spin Hall effects can be observed in inhomogeneous media and at optical interfaces[12]. Spin-orbital Hall effect is obtained when an asymmetric light beam possessing spin or orbital angular momentum (SAM/OAM) is tightly focused and the effect is manifested in a shift of barycenter/center of gravity of light in the transverse focal plane. Here an asymmetric beam is assumed to be either a beam which loses its symmetry by partial masking/obstruction or a beam shifted from the optical axis. A linearly polarized asymmetric input beam has an electric field

[1]Image Processing Systems Institute of RAS—Branch of the FSRC "Crystallography and Photonics" RAS, Samara 443001, Russia; [2]School of Advanced Technology, Algonquin College, Ottawa, Ontario K2G 1V8, Canada.

*Correspondence: A Porfirev, E-mail: porfirev.alexey@gmail.com

Received: 7 June 2023; Accepted: 20 July 2023; Published online: 27 September 2023

distribution in the focal plane containing (new) transverse and longitudinal components which possess elements of symmetry due to diffraction[13], and thus the focal distribution differs significantly from that of the input beam. An asymmetric input beam with spin and/or OAM will obviously have a non-uniform input angular momentum (AM) with transverse and longitudinal components[8,9]. Since the AM components depend on electric field components, the focal plane electric field distribution has to reflect/accommodate the presence/conservation of AM and thus has to differ from the symmetrical focal plane distribution exhibited when focusing a linear polarized asymmetric input beam. This is achieved by shifts of the barycenters of the field components in the focus in order to produce the required AM components.

In some more detail, a spatially asymmetric optical beam with helicity (OAM) and/or handedness (spin) has an external OAM, $\boldsymbol{L}^{\rm ext}\propto(\boldsymbol{r}\times\boldsymbol{p})$, where $\boldsymbol{r}$ is the radius and $\boldsymbol{p}\propto\mathrm{Re}(\boldsymbol{E}^*\times\boldsymbol{H})$ is the linear momentum, and $\boldsymbol{E}$ and $\boldsymbol{H}$ are electric and magnetic fields. Due to the conservation of angular momentum this necessitates, upon tight focusing, the appearance of this external OAM in the focal plane[8,9,14]. For example, the longitudinal component of this OAM is $L_z^{\rm ext}\propto xp_y-yp_x\propto xE_z^*E_x-yE_y^*E_z$, and from this relation the simplest and foremost way for the light to generate this component in the focal plane is to have an asymmetric distribution/shift of the "new" (absent in the input) component, E_z. The shift of the z component of the field was first shown by Baranova et al.[6] and it is this field component whose shift is studied in most of the subsequent publications on spin Hall effect of light upon focusing. Similar arguments can be invoked in relation to the SAM: the asymmetric input beam after the lens has both transverse and longitudinal SAM components expressed by $E_i^*E_j$, and this also requires corresponding shifts in the electric field distribution in the focal plane. Thus, the light has to "self-organize" or restructure itself in the focus to satisfy angular momentum conservation law. The above deliberations point at the importance of knowing the distribution of different components of the focused asymmetric input beam possessing spin and/or vorticity. Since the azimuthal/cylindrical symmetry of the system is broken, it is prudent to study the Hall effect of light upon tight focusing in the Cartesian coordinates as opposed to cylindrical ones as is done in most previous studies. Precisely this was performed in ref.[10] for an asymmetric input beam with spin, where it was shown that different Cartesian components shift by different amounts and in opposite ways perpendicular to the direction of symmetry breaking. In the present work, we expand the study to include input beams with OAM as well as with spin/OAM simultaneously. While these cases are more complicated, a similar picture displaying different shifts of different components is exhibited. We also relate the electric field shifts to the shifts of spin or OAM components and in addition to well-known spin-orbit and orbit-orbit conversion in Hall effect of light upon focusing we show occurrence of orbit-spin conversion. Experimental results performed in azopolymers confirm our findings.

Theoretical analysis

We shall perform the calculation for the case when the input field $B(\alpha, \beta)$ is given in the spatial frequency domain in Cartesian coordinates (see Fig. 1(a)). The Richards-Wolf formulas[15] thus acquire the following form[16–18]:

$$\boldsymbol{E}(u,v,z)=-\frac{\mathrm{i}f}{\lambda}\iint\limits_{\Omega=[-1,1]}B(\alpha,\beta)\boldsymbol{P}(\alpha,\beta)\cdot\exp\left\{\mathrm{i}k\left[\alpha u+\beta v+z\sqrt{1-\left(\alpha^2+\beta^2\right)}\right]\right\}\mathrm{d}\alpha\,\mathrm{d}\beta\,,\quad(1)$$

where $k = 2\pi/\lambda$ is the wave vector of radiation with a wavelength λ, (α, β) are spatial frequencies (dimensionless quantities) for propagating waves $\alpha^2 + \beta^2 \le 1$, and $\gamma=\sqrt{1-\left(\alpha^2+\beta^2\right)}$.

Polarization transformation of the input field with an uniform polarization state $\boldsymbol{c}=\begin{bmatrix}c_x\\c_y\end{bmatrix}$ is described by an expression[19]:

$$\boldsymbol{P}(\alpha,\beta)=\frac{1}{\alpha^2+\beta^2}\cdot\begin{bmatrix}\beta^2+\alpha^2\gamma & -\alpha\beta(1-\gamma)\\ -\alpha\beta(1-\gamma) & \alpha^2+\beta^2\gamma\\ -\alpha\left(\alpha^2+\beta^2\right) & -\beta\left(\alpha^2+\beta^2\right)\end{bmatrix}\begin{bmatrix}c_x\\c_y\end{bmatrix}.\quad(2)$$

Then Eq. (1) can be written in the following form:

$$\boldsymbol{E}(u,v,0)=-\frac{\mathrm{i}f}{\lambda}\iint\limits_{\Omega}\frac{B(\alpha,\beta)}{\alpha^2+\beta^2}\cdot\begin{pmatrix}c_x(\beta^2+\alpha^2\gamma)-c_y\alpha\beta(1-\gamma)\\ -c_x\alpha\beta(1-\gamma)+c_y(\alpha^2+\beta^2\gamma)\\ -(\alpha^2+\beta^2)(c_x\alpha+c_y\beta)\end{pmatrix}\cdot\exp\left\{\mathrm{i}k\left[\alpha u+\beta v\right]\right\}\mathrm{d}\alpha\mathrm{d}\beta\,.\quad(3)$$

From a mathematical point of view, Eq. (3) is the Fourier transform of the function $B(\alpha, \beta)$ weighted by a superposition of coordinates. We denote the Fourier

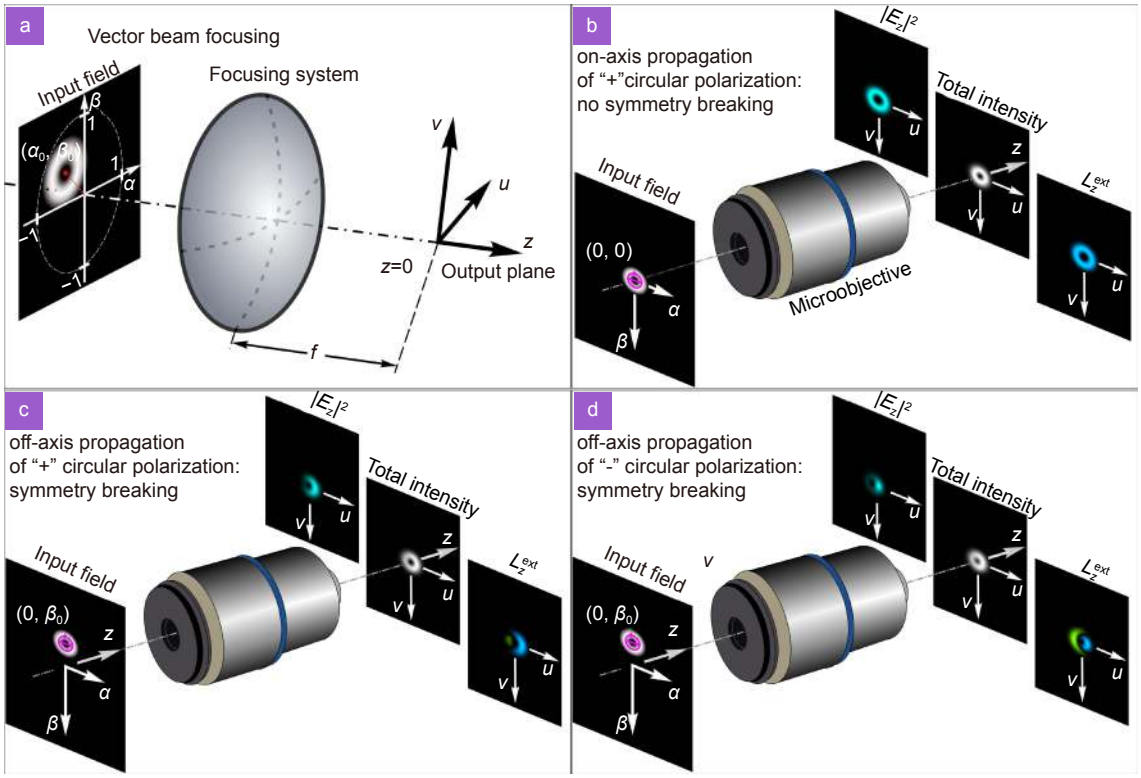

Fig. 1 | Numerical investigation of vectorial spin-orbital Hall effect of light upon tight focusing: (**a**) spatial frequency domain in Cartesian coordinates, (**b–d**) on- and off-axis propagation of a circularly polarized first-order optical vortex beam. The symmetry breaking in the longitudinal component and extrinsic OAM L_z^{ext} are shown.

transform of the function $B(\alpha, \beta)$ as follows:

$$\Phi(u,v) = \Im\left[B(\alpha,\beta)\right] = A_0 \iint\limits_{\Omega} B(\alpha,\beta) \cdot \exp\left\{\mathrm{i}k\left[\alpha u + \beta v\right]\right\} \mathrm{d}\alpha\,\mathrm{d}\beta\,. \tag{4}$$

If $\Phi(u, v)$ is known in an analytical form, then one can try to obtain an analytical expression for Eq. (3). In particular, the simplest expression is obtained for the longitudinal component of the focused field of Eq. (3) as a superposition of the corresponding partial derivatives of $\Phi(u, v)$:

$$\begin{aligned} E_z(u,v,0) &= \frac{\mathrm{i}f}{\lambda} \iint\limits_{\Omega} B(\alpha,\beta)\left(c_x\alpha + c_y\beta\right) \cdot \exp\left\{\mathrm{i}k\left[\alpha u + \beta v\right]\right\} \mathrm{d}\alpha\,\mathrm{d}\beta \\ &\approx A_0\left(c_x\frac{\partial\Phi(u,v)}{\partial u} + c_y\frac{\partial\Phi(u,v)}{\partial v}\right), \end{aligned} \tag{5}$$

where the coefficient A_0 has the dimension of length and was introduced to compensate for the action of derivatives.

Let the input field be a shifted single-ring vortex Laguerre-Gauss (LG) mode:

$$B(\alpha,\beta) = LG_{0m}\left(\alpha-\alpha_0, \beta-\beta_0\right), \tag{6}$$

where (α_0, β_0) are offset parameters, $LG_{0m}(\alpha_0, \beta_0)$ is the LG mode[20–22]:

$$LG_{0m}(\alpha,\beta) = \sqrt{\frac{2}{\pi|m|!}}\exp\left(-\frac{\alpha^2+\beta^2}{w_s^2}\right) \cdot \left(\frac{\sqrt{2}\left[\alpha + \mathrm{isgn}(m)\beta\right]}{w_s}\right)^{|m|}, \tag{7}$$

where the parameter w_s is dimensionless since Eq. (7) corresponds to the spatial frequency plane.

It is known that LG modes are invariant to the Fourier transform[23,24], therefore:

$$\Phi(u,v) \approx A_0\exp\left[\mathrm{i}k\left(\alpha_0 u + \beta_0 v\right)\right] LG_{0m}(u,v), \tag{8}$$

where $LG_{0m}(u, v)$ is LG mode in the spatial domain:

$$LG_{0m}(u,v) = \sqrt{\frac{2}{\pi|m|!}}\exp\left(-\frac{u^2+v^2}{w_0^2}\right) \cdot \left(\frac{\sqrt{2}\left[u + \mathrm{isgn}(m)v\right]}{w_0}\right)^{|m|}, \tag{9}$$

where (u, v) and $w_0 = \lambda(\pi w_s)^{-1}$ have length dimension.

It should be noted that in the paraxial case, when the numerical aperture of the focusing system is small, then $\alpha^2 + \beta^2 << 1$, $\gamma \to 1$, and Eq. (2) is greatly simplified and reduced to the form:

$$\boldsymbol{P}(\alpha,\beta)\approx\begin{bmatrix}1&0\\0&1\\-\alpha&-\beta\end{bmatrix}\begin{bmatrix}c_x\\c_y\end{bmatrix}. \tag{10}$$

Thus, in this case, the transverse components of the field in the focal plane will be determined in accordance with Eq. (8), i.e. the intensity for the Fourier-invariant beams will not change when the original field is shifted. The effect of asymmetry remains just in the longitudinal component, however, its contribution will become insignificant. It follows from the above that in order to obtain a noticeable vector effect, the numerical aperture of the focusing system should be significant (NA>0.4).

Rigorous analysis for the longitudinal component

From previous deliberations, the longitudinal component in the focal plane for the shifted LG mode can be calculated explicitly:

$$E_z(u,v,0)\approx\frac{\mathrm{i}}{k}\left(c_x\frac{\partial}{\partial u}+c_y\frac{\partial}{\partial v}\right)\cdot\left\{\exp\left[\mathrm{i}k\left(\alpha_0u+\beta_0v\right)\right]LG_{0m}(u,v)\right\}. \tag{11}$$

The derivatives in Eq. (11) have the form:

$$\begin{aligned}\frac{\partial}{\partial u}\{\cdot\}=&\exp\left[\mathrm{i}k\left(\alpha_0u+\beta_0v\right)\right]\\&\cdot\left\{\mathrm{i}k\alpha_0LG_{0m}(u,v)+\frac{\partial}{\partial u}LG_{0m}(u,v)\right\},\\\frac{\partial}{\partial v}\{\cdot\}=&\exp\left[\mathrm{i}k\left(\alpha_0u+\beta_0v\right)\right]\\&\cdot\left\{\mathrm{i}k\beta_0LG_{0m}(u,v)+\frac{\partial}{\partial v}LG_{0m}(u,v)\right\}.\end{aligned} \tag{12}$$

Using Eq. (9), we obtain derivatives of LG modes:

$$\begin{aligned}\frac{\partial}{\partial u}LG_{0m}(u,v)=&\frac{A_1}{w_0}\exp\left(-\frac{u^2+v^2}{w_0^2}\right)\left[\frac{u+\mathrm{isgn}(m)v}{w_0}\right]^{|m|-1}\\&\cdot\left[-\frac{2u}{w_0^2}\left(u+\mathrm{isgn}(m)v\right)+|m|\right],\\\frac{\partial}{\partial v}LG_{0m}(u,v)=&\frac{A_1}{w_0}\exp\left(-\frac{u^2+v^2}{w_0^2}\right)\left[\frac{u+\mathrm{isgn}(m)v}{w_0}\right]^{|m|-1}\\&\cdot\left[-\frac{2v}{w_0^2}\left(u+\mathrm{isgn}(m)v\right)+\mathrm{isgn}(m)\,|m|\right],\end{aligned} \tag{13}$$

where $A_1=\frac{\mathrm{i}}{k}\left(\sqrt{2}\right)^{|m|}\sqrt{\frac{2}{\pi\,|m|!}}$.

We substitute Eq. (13) into Eq. (12) and then into Eq. (11). As a result, we get:

$$\begin{aligned}E_z(u,v,0)\approx&\,c_x\cdot E_1+c_y\cdot E_2,\\E_1=&\exp\left[\mathrm{i}k\left(\alpha_0u+\beta_0v\right)\right]\\&\cdot\frac{A_1}{w_0}\exp\left(-\frac{u^2+v^2}{w_0^2}\right)\left[\frac{u+\mathrm{isgn}(m)v}{w_0}\right]^{|m|-1}\\&\cdot\left[\left(u+\mathrm{isgn}(m)v\right)\left(\mathrm{i}k\alpha_0-\frac{2u}{w_0^2}\right)+|m|\right],\\E_2=&\exp\left[\mathrm{i}k\left(\alpha_0u+\beta_0v\right)\right]\\&\cdot\frac{A_1}{w_0}\exp\left(-\frac{u^2+v^2}{w_0^2}\right)\left[\frac{u+\mathrm{isgn}(m)v}{w_0}\right]^{|m|-1}\\&\cdot\left[\left(u+\mathrm{isgn}(m)v\right)\left(\mathrm{i}k\beta_0-\frac{2v}{w_0^2}\right)+\mathrm{isgn}(m)\,|m|\right].\end{aligned} \tag{14}$$

Note that Eq. (14) are also valid for m = 0, in this case:

$$\begin{aligned}E_1(m=0)=&\exp\left[\mathrm{i}k\left(\alpha_0u+\beta_0v\right)\right]\\&\cdot A_1\exp\left(-\frac{u^2+v^2}{w_0^2}\right)\cdot\left(\mathrm{i}k\alpha_0-\frac{2u}{w_0^2}\right),\\E_2(m=0)=&\exp\left[\mathrm{i}k\left(\alpha_0u+\beta_0v\right)\right]\\&\cdot A_1\exp\left(-\frac{u^2+v^2}{w_0^2}\right)\cdot\left(\mathrm{i}k\beta_0-\frac{2v}{w_0^2}\right).\end{aligned} \tag{15}$$

Equations (15) coincide with those that can be derived if we substitute m = 0 directly into Eq. (11).

From Eq. (14) one can obtain expression for the intensity:

$$\begin{aligned}|E_z(u,v,0)|^2=&\left(\frac{A_1}{w_0}\right)^2\exp\left(-2\frac{u^2+v^2}{w_0^2}\right)\left(\frac{u^2+v^2}{w_0^2}\right)^{|m|-1}\\\times&\left|c_x\left[\left(u+\mathrm{isgn}(m)v\right)\left(\mathrm{i}k\alpha_0-\frac{2u}{w_0^2}\right)+|m|\right]\right.\\&\left.+c_y\left[\left(u+\mathrm{isgn}(m)v\right)\left(\mathrm{i}k\beta_0-\frac{2v}{w_0^2}\right)+\mathrm{isgn}(m)\,|m|\right]\right|^2.\end{aligned} \tag{16}$$

As seen from Eq. (16), there is a significant dependence on the initial polarization. The differences between the two situations should be especially noticeable: the first corresponds to linear polarization (both values c_x, c_y are real), and the second is associated with elliptical polarization (when c_x is real and c_y is purely imaginary).

Approximate analysis for transverse components

Expressions in Eq. (3) for the transverse components are much more complex. Therefore, in order to obtain analytical expressions convenient for further analysis, we shall assume that most of the energy is concentrated on the peripheral area with high frequencies $\left(\alpha^2+\beta^2\right)\to1$, which corresponds to $\gamma\to0$. Then from Eq. (3), we obtain a simpler expressions for the transverse components:

$$\boldsymbol{E}_{\perp}(u,v,0) = -\frac{\mathrm{i}f}{\lambda}\iint_{\Omega} B(\alpha,\beta)\,(c_x\beta - c_y\alpha)\begin{pmatrix}\beta\\ -\alpha\end{pmatrix} \cdot \exp\{\mathrm{i}k\,[\alpha u+\beta v]\}\,\mathrm{d}\alpha\,\mathrm{d}\beta\,. \tag{17}$$

From Eq. (17) one can get

$$\begin{aligned} E_x(u,v,0) &= -\frac{1}{k^2}\left(c_x\frac{\partial^2}{\partial v^2} - c_y\frac{\partial^2}{\partial u\partial v}\right)\\ &\cdot\left\{\exp\left[\mathrm{i}k\left(\alpha_0 u+\beta_0 v\right)\right]LG_{0m}(u,v)\right\},\\ E_y(u,v,0) &= -\frac{1}{k^2}\left(-c_x\frac{\partial^2}{\partial u\partial v} + c_y\frac{\partial^2}{\partial u^2}\right)\\ &\cdot\left\{\exp\left[\mathrm{i}k\left(\alpha_0 u+\beta_0 v\right)\right]LG_{0m}(u,v)\right\}\,. \end{aligned} \tag{18}$$

The second derivatives are obtained by repeated differentiation of the expressions from Eq. (14):

$$\begin{aligned} &\frac{\partial^2}{\partial u^2}(\ldots) = \exp\left[\mathrm{i}k\left(\alpha_0 u+\beta_0 v\right)\right]\exp\left(-\frac{u^2+v^2}{w_0^2}\right)\\ &\cdot(u+\mathrm{isgn}(m)v)^{|m|-2}\times\{(|m|-1)|m| + 2\mathrm{i}|m|\,k\alpha_0(u\pm\mathrm{i}v)\\ &-k^2\alpha_0^2(u\pm\mathrm{i}v)^2 + \frac{2}{w_0^2}\left[-(2|m|+1)u^2+v^2-2\mathrm{isgn}(m)\right.\\ &\left.\cdot(|m|+1)uv\right] - \frac{4\mathrm{i}k\alpha_0}{w_0^2}u(u\pm\mathrm{i}v)^2 + \frac{4}{w_0^4}u^2(u\pm\mathrm{i}v)^2\Big\}, \end{aligned} \tag{19}$$

$$\begin{aligned} &\frac{\partial^2}{\partial v^2}(\ldots) = \exp\left[\mathrm{i}k\left(\alpha_0 u+\beta_0 v\right)\right]\exp\left(-\frac{u^2+v^2}{w_0^2}\right)\\ &\cdot(u+\mathrm{isgn}(m)v)^{|m|-2}\times\{-(|m|-1)|m| - 2mk\beta_0(u\pm\mathrm{i}v)\\ &-k^2\beta_0^2(u\pm\mathrm{i}v)^2 + \frac{2}{w_0^2}\left[-u^2+(2|m|+1)v^2-2\mathrm{isgn}(m)\right.\\ &\left.\cdot(|m|+1)uv\right] - \frac{4\mathrm{i}k\beta_0}{w_0^2}v(u\pm\mathrm{i}v)^2 + \frac{4}{w_0^4}v^2(u\pm\mathrm{i}v)^2\Big\}. \end{aligned} \tag{20}$$

It can be seen that there is some correspondence of symmetry between Eqs. (19) and (20). The expression for the mixed derivative also reveals a certain similarity, while it equally contains α_0 and β_0:

$$\begin{aligned} &\frac{\partial^2}{\partial u\partial v}(\ldots) = \exp\left[\mathrm{i}k\left(\alpha_0 u+\beta_0 v\right)\right]\exp\left(-\frac{u^2+v^2}{w_0^2}\right)\\ &\cdot(u+\mathrm{isgn}(m)v)^{|m|-2}\times\{\mathrm{i}m(|m|-1) - mk\alpha_0(u\pm\mathrm{i}v)\\ &+\mathrm{i}|m|\,k\beta_0(u\pm\mathrm{i}v) - k^2\alpha_0\beta_0(u\pm\mathrm{i}v)^2 - \frac{2\mathrm{i}m}{w_0^2}(u^2+v^2)\\ &-\frac{2\mathrm{i}k\alpha_0}{w_0^2}v(u\pm\mathrm{i}v)^2 - \frac{2\mathrm{i}k\beta_0}{w_0^2}u(u\pm\mathrm{i}v)^2 + \frac{4}{w_0^4}uv(u\pm\mathrm{i}v)^2\Big\}. \end{aligned} \tag{21}$$

In Eqs. (19–21) we omit factors which do not depend on variables u and v. If we take them into account and denote $A_2 = -\frac{1}{k^2}(\sqrt{2})^{|m|}\sqrt{\frac{2}{\pi|m|!}}$, then after substitution Eqs. (19–21) into Eq. (18) , we finally get:

$$\begin{aligned} E_x(u,v,0) =& \exp\left[\mathrm{i}k\left(\alpha_0 u+\beta_0 v\right)\right]\cdot\frac{A_2}{w_0^2}\cdot\exp\left(-\frac{u^2+v^2}{w_0^2}\right)\\ &\cdot\left[\frac{u+\mathrm{isgn}(m)v}{w_0}\right]^{|m|-2}\cdot\left[c_x D_{vv} - c_y D_{uv}\right],\\ E_y(u,v,0) =& \exp\left[\mathrm{i}k\left(\alpha_0 u+\beta_0 v\right)\right]\cdot\frac{A_2}{w_0^2}\cdot\exp\left(-\frac{u^2+v^2}{w_0^2}\right)\\ &\cdot\left[\frac{u+\mathrm{isgn}(m)v}{w_0}\right]^{|m|-2}\cdot\left[-c_x D_{uv} + c_y D_{uu}\right]. \end{aligned} \tag{22}$$

where D_{uu}, D_{vv}, D_{uv} denote expressions in curly brackets from Eqs. (19–21), respectively. The intensity of the transverse components have the following form:

$$\begin{aligned} |E_x(u,v,0)|^2 &= \left(\frac{A_2}{w_0^2}\right)^2\exp\left(-2\frac{u^2+v^2}{w_0^2}\right)\\ &\cdot\left(\frac{u^2+v^2}{w_0^2}\right)^{|m|-2}\cdot|c_x D_{vv} - c_y D_{uv}|^2,\\ |E_y(u,v,0)|^2 &= \left(\frac{A_2}{w_0^2}\right)^2\exp\left(-2\frac{u^2+v^2}{w_0^2}\right)\\ &\cdot\left(\frac{u^2+v^2}{w_0^2}\right)^{|m|-2}\cdot|-c_x D_{uv} + c_y D_{uu}|^2. \end{aligned} \tag{23}$$

Also, there is a significant dependence on the initial polarization. In the next section, we consider several characteristic cases of analytical expressions for linear and circular polarization of the input field and perform numerical calculations based on Eq. (1) without any approximations.

As follows from our analytical results, the magnitude of the shift is important, the larger α_0 or β_0 (depending on the polarization), the more noticeable the effect will be, i.e. the asymmetry will be more pronounced.

Numerical calculations and comparative analysis

In this section, a comparative numerical simulation is performed for the input field in the form of a single-ring vortex LG mode of Eqs. (6–7) with linear and circular polarization for different values of vortex order m. Numerical calculations are performed on the basis of Eq. (1) without any approximations (see Fig. 1(b–d)). The calculation parameters are as follows: lens radius 100λ, focal length $f = 101\lambda$, $NA = 0.99$, $w_s = 0.15$, α_0=0, β_0=0.5.

The Figs. 2–7 below show the intensity distribution patterns in the focal plane. The intensity of x, y, z components ($|E_x|^2$, $|E_y|^2$, $|E_z|^2$) are in red, green, and blue, respectively, total intensity $|\boldsymbol{E}|^2$ is shown in grayscale.

We also calculate the SAM $\boldsymbol{s}$ and extrinsic OAM $\boldsymbol{L}_{\mathrm{ext}}$[8]:

$$\boldsymbol{s}=\begin{pmatrix} s_x \\ s_y \\ s_z \end{pmatrix} \propto \mathrm{Im}\begin{pmatrix} E_y^*E_z - E_z^*E_y \\ E_z^*E_x - E_x^*E_z \\ E_x^*E_y - E_y^*E_x \end{pmatrix} = 2\mathrm{Im}\begin{pmatrix} E_y^*E_z \\ E_z^*E_x \\ E_x^*E_y \end{pmatrix}. \tag{24}$$

$$\boldsymbol{L}^{\mathrm{ext}}=\begin{pmatrix} L_x^{\mathrm{ext}} \\ L_y^{\mathrm{ext}} \\ L_z^{\mathrm{ext}} \end{pmatrix} \propto (\boldsymbol{r}\times\boldsymbol{p}) = \begin{pmatrix} yp_z - zp_y \\ zp_x - xp_z \\ xp_y - yp_x \end{pmatrix}, \tag{25}$$

where $\boldsymbol{p}\propto\mathrm{Re}(\boldsymbol{E}^*\times\boldsymbol{H})$ is the linear momentum.

For $\boldsymbol{L}^{\mathrm{ext}}$ we have at the focal plane ($z = 0$):

$$\boldsymbol{L}^{\mathrm{ext}}(z=0) \propto \begin{pmatrix} yp_z \\ -xp_z \\ xp_y - yp_x \end{pmatrix}. \tag{26}$$

Figure 2 also show all the components of SAM (a light color for positive values and a dark color for negative values) and the longitudinal component $L_z^{\mathrm{ext}} \propto xp_y - yp_x$ (orange color for positive values and violet color for negative values). The transverse components of L_x^{ext}, L_y^{ext} were also calculated but their average is zero, they are not shifted and thus of no interest in this work.

Linear *x*-polarization of the input field (c_x = 1, c_y = 0)

In this case, using Eq. (16), we obtain the following expression for the longitudinal component in the focal plane:

$$\left|E_z^{\mathrm{lin}\,x}(u,v,0)\right|^2 = I_m(u,v)\left[\left(\frac{2u^2}{w_0^2} + \mathrm{sgn}(m)k\alpha_0 v - |m|\right)^2 + \left(k\alpha_0 u - \mathrm{sgn}(m)\frac{2uv}{w_0^2}\right)^2\right], \tag{27}$$

where $I_m(u, v)$ is a multiplier independent of polarization.

As follows from Eq. (27), there is a dependence on α_0, but no dependence on β_0, i.e., only the displacement of the input field along the axis coinciding with the polarization axis affects the distortion of the intensity of the longitudinal component.

Note, in the horizontal intensity section (at v = 0, along the u coordinate) there is no asymmetry:

$$\left|E_z^{\mathrm{lin}\,x}(u,0,0)\right|^2 = I_m(u,0)\left[\left(\frac{2u^2}{w_0^2} - |m|\right)^2 + k^2\alpha_0^2u^2\right], \tag{28}$$

however, in the vertical section (at u = 0, along the v coordinate) there is an asymmetry associated with the horizontal displacement α_0 and the vortex number $|m|$:

$$\left|E_z^{\mathrm{lin}\,x}(0,v,0)\right|^2 = I_m(0,v)\left(\mathrm{sgn}(m)k\alpha_0 v - |m|\right)^2. \tag{29}$$

As can be seen from Eq. (29), the direction of the optical vortex, i.e. the sgn(m) affects only the change in the direction of the asymmetry (maximum in the upper or lower part).

The expressions for the transverse components are rather complex even in the approximate form of Eq. (23), so we write only their horizontal and vertical sections:

$$\left|E_x^{\mathrm{lin}\,x}(u,0,0)\right|^2 = I_m(u,0)\cdot\left[\left(k^2\beta_0^2 + \frac{2}{w_0^2}\right)u^2 + 2mk\beta_0 u + (|m|-1)|m|\right]^2. \tag{30}$$

$$\left|E_x^{\mathrm{lin}\,x}(0,v,0)\right|^2 = I_m(0,v)\cdot\left\{\left[\frac{4}{w_0^4}v^4 - \left(k^2\beta_0^2 + \frac{2}{w_0^2}(2|m|+1)\right)v^2 + (|m|-1)|m|\right]^2 + 4k^2\beta_0^2v^2\left(\frac{2v^2}{w_0^2} - |m|\right)^2\right\}. \tag{31}$$

Note, the focal intensity distribution of the x-component, in contrast to the z-component, is affected only by the vertical shift β_0 of the input field. Moreover, the vertical section is much more complicated than the horizontal one. At the same time, the focal intensity distribution of the y-component depends on both α_0 and β_0. Corresponding sections are very similar:

$$\left|E_y^{\mathrm{lin}\,x}(u,0,0)\right|^2 = I_m(u,0)\left\{k^2\alpha_0^2u^2(k\beta_0u+m)^2 + \left[\frac{2k\beta_0}{w_0^2}u^3 + \frac{2m}{w_0^2}u^2 - |m|\,k\beta_0u - (|m|-1)m\right]^2\right\}. \tag{32}$$

$$\left|E_y^{\mathrm{lin}\,x}(0,v,0)\right|^2 = I_m(0,v)\left\{k^2\beta_0^2v^2(k\alpha_0v-m)^2 + \left[\frac{2k\alpha_0}{w_0^2}v^3 - \frac{2m}{w_0^2}v^2 - |m|\,k\alpha_0v + (|m|-1)m\right]^2\right\}. \tag{33}$$

The results of focusing simulation for the x-linearly polarized field, both in the absence of a shift and with a vertical shift (α_0=0, β_0=0.5), for various values of m are shown in Figs. 2–3. In full accordance with the theoretical calculations, the z-component is not distorted (since α_0=0), the transverse components are noticeably deformed, and the center of gravity shifts in different directions when the sign of m changes. An increase in the vortex order m leads to a scale increase in the formed patterns.

Linear *y*-polarization of the input field (c_x = 0, c_y = 1)

In this case, we obtain the following expression for the longitudinal component in the focal plane:

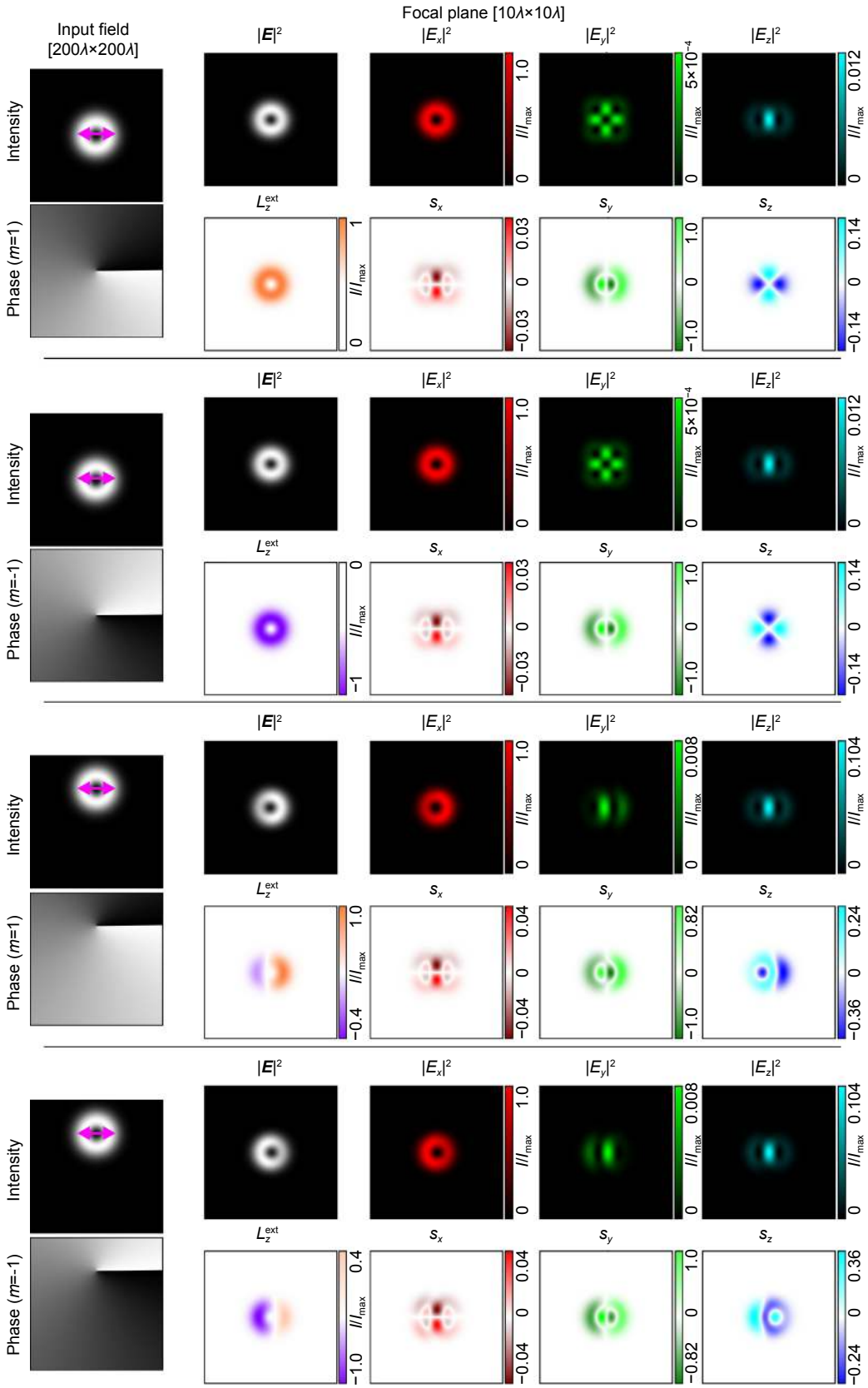

Fig. 2 | Comparison of asymmetry in focusing a shifted vortex beam with *m*=±1 order for *x*-linear polarization.

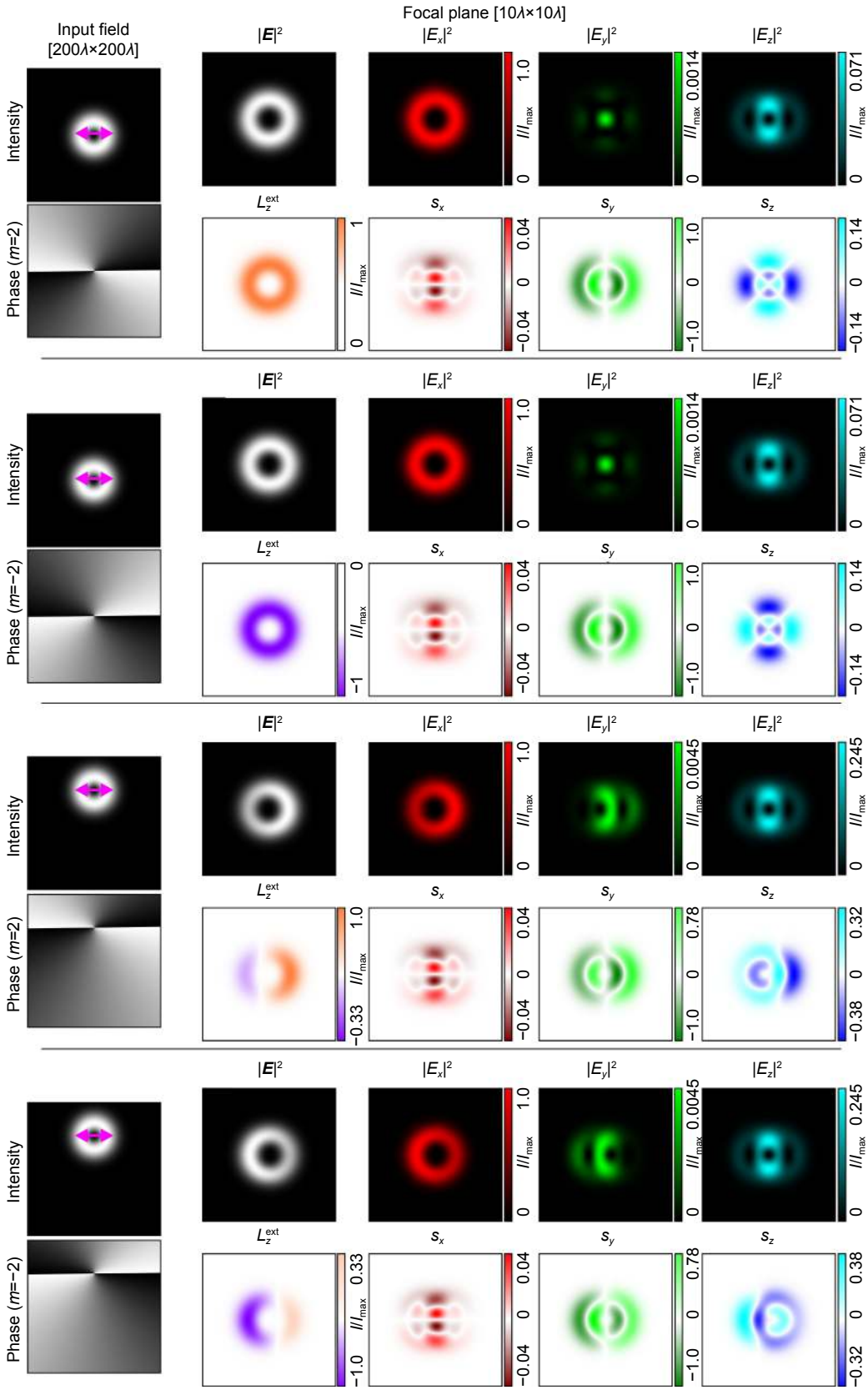

Fig. 3 | Comparison of asymmetry in focusing a shifted vortex beam with *m*=±2 order for *x*-linear polarization.

$$\left|E_z^{\text{lin}\,y}(u,v,0)\right|^2 = I_m(u,v)\left[\left(\text{sgn}(m)k\beta_0 v + \frac{2uv}{w_0^2}\right)^2 + \left(-\text{sgn}(m)\frac{2v^2}{w_0^2} + k\beta_0 u + \text{sgn}(m)\,|m|\right)^2\right]. \quad (34)$$

In contrast to the previous case, there is a dependence only on β_0, that is, also, only the displacement of the input field along the axis coinciding with the polarization axis has an effect on the distortion of the intensity of the longitudinal component.

In the horizontal intensity cross section (at v = 0), there is an asymmetry associated with the value β_0 and the vortex number m (sgn(m) only affects the change in the direction of the asymmetry):

$$\left|E_z^{\text{lin}\,y}(u,0,0)\right|^2 = I_m(u,0)\left(k\beta_0 u + m\right)^2. \quad (35)$$

There is no asymmetry in the vertical section:

$$\left|E_z^{\text{lin}\,y}(0,v,0)\right|^2 = I_m(0,v)\left[k^2\beta_0^2 v^2 + \left(\frac{2v^2}{w_0^2} - |m|\right)^2\right]. \quad (36)$$

There is also an analogy with the previous case for transverse components, however, they change places. In particular, the x-component coincides with the y-component from Section *Linear x-polarization of the input field* (see Eqs. (32, 33)), and the focal intensity distribution for the y-component depends only on the input field displacement in the horizontal direction α_0:

$$\left|E_y^{\text{lin}\,y}(u,0,0)\right|^2 = I_m(u,0)\left\{\left[\frac{4}{w_0^4}u^4 - \left(k^2\alpha_0^2 + \frac{2}{w_0^2}\cdot(2|m|+1)\right)u^2 + (|m|-1)|m|\right]^2 + 4k^2\alpha_0^2u^2\left(\frac{2u^2}{w_0^2} - |m|\right)^2\right\}. \quad (37)$$

$$\left|E_y^{\text{lin}\,y}(0,v,0)\right|^2 = I_m(0,v)\left[\left(k^2\alpha_0^2 + \frac{2}{w_0^2}\right)v^2 - 2mk\alpha_0 v + (|m|-1)|m|\right]^2. \quad (38)$$

The results of focusing simulation for a y-linearly polarized field both in the absence of perturbation and with a vertical shift (α_0= 0, β_0=0.5), for various values of m are shown in Figs. 4–5. The simulation results confirm the analytical calculations. In this case, the input field shift along the polarization axis affects the distortion of both transverse and longitudinal components. The impact gets more complex. We note that in the case of tight focusing, the asymmetry of the total intensity depends significantly on the contribution of the z-component.

Linear diagonal polarization of the input field ($c_x = c_y = 1/\sqrt{2}$)

This variant actually combines the two previous ones, so the focal distribution of the intensity of the longitudinal component depends on both the horizontal α_0 and vertical β_0 displacements of the input field:

$$\left|E_z^{\text{lin}\,xy}(u,v,0)\right|^2 = I_m(u,v)\cdot\left[\left(\frac{2u}{w_0^2}(u+v) + \text{sgn}(m)k(\alpha_0+\beta_0)v - |m|\right)^2 + \left(k(\alpha_0+\beta_0)u - \text{sgn}(m)\frac{2v}{w_0^2}(u+v) + \text{sgn}(m)\,|m|\right)^2\right]. \quad (39)$$

The corresponding sections have the following form:

$$\left|E_z^{\text{lin}\,xy}(u,0,0)\right|^2 = I_m(u,0)\cdot\left[\left(\frac{2u^2}{w_0^2} - |m|\right)^2 + \left(k(\alpha_0+\beta_0)u + \text{sgn}(m)\,|m|\right)^2\right], \quad (40)$$

$$\left|E_z^{\text{lin}\,xy}(0,v,0)\right|^2 = I_m(0,v)\cdot\left[\left(\text{sgn}(m)k(\alpha_0+\beta_0)v - |m|\right)^2 + \left(\frac{2v^2}{w_0^2} - |m|\right)^2\right]. \quad (41)$$

It can be seen from the above expressions that there is a dependence only on the sum (α_0 + β_0). Using the general Eq. (16), one can verify that for linear polarization (i.e. real c_x, c_y) the intensity will depend not separately on α_0 or β_0, but on the combination $c_x\alpha_0$ + $c_y\beta_0$. Therefore, to simplify measurements, it is more convenient to use polarization along one axis with the corresponding displacements. The distribution of the transverse components will also represent the hybrid form.

Circular "+"-polarization of the input field ($c_x = 1/\sqrt{2}$, $c_y = \mathrm{i}/\sqrt{2}$)

This case differs significantly from those considered above. Based on Eq. (16), the intensity distribution of the longitudinal component in the focal plane has the following form:

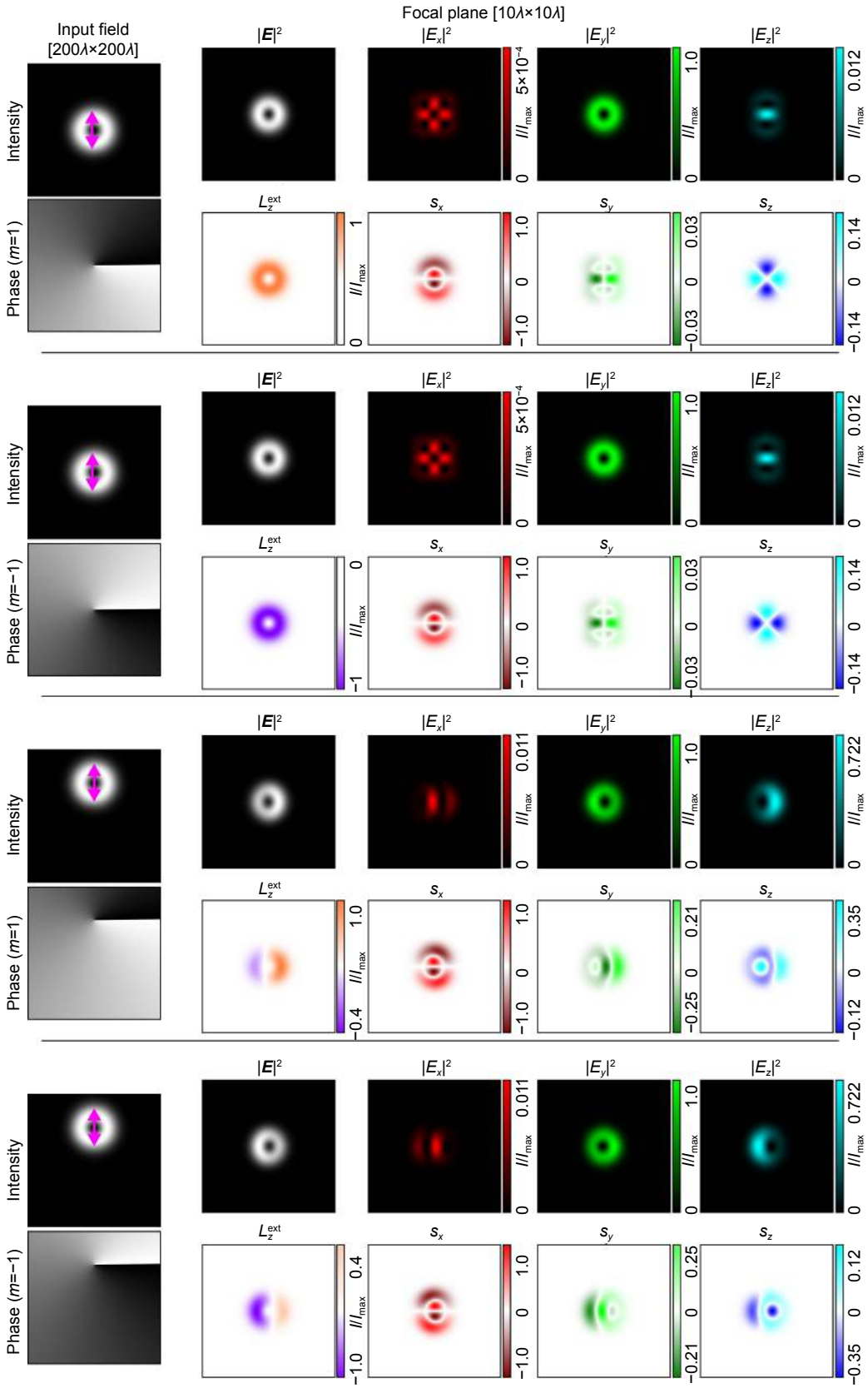

Fig. 4 | Comparison of asymmetry in focusing a shifted vortex beam with *m*=±1 order for *y*-linear polarization.

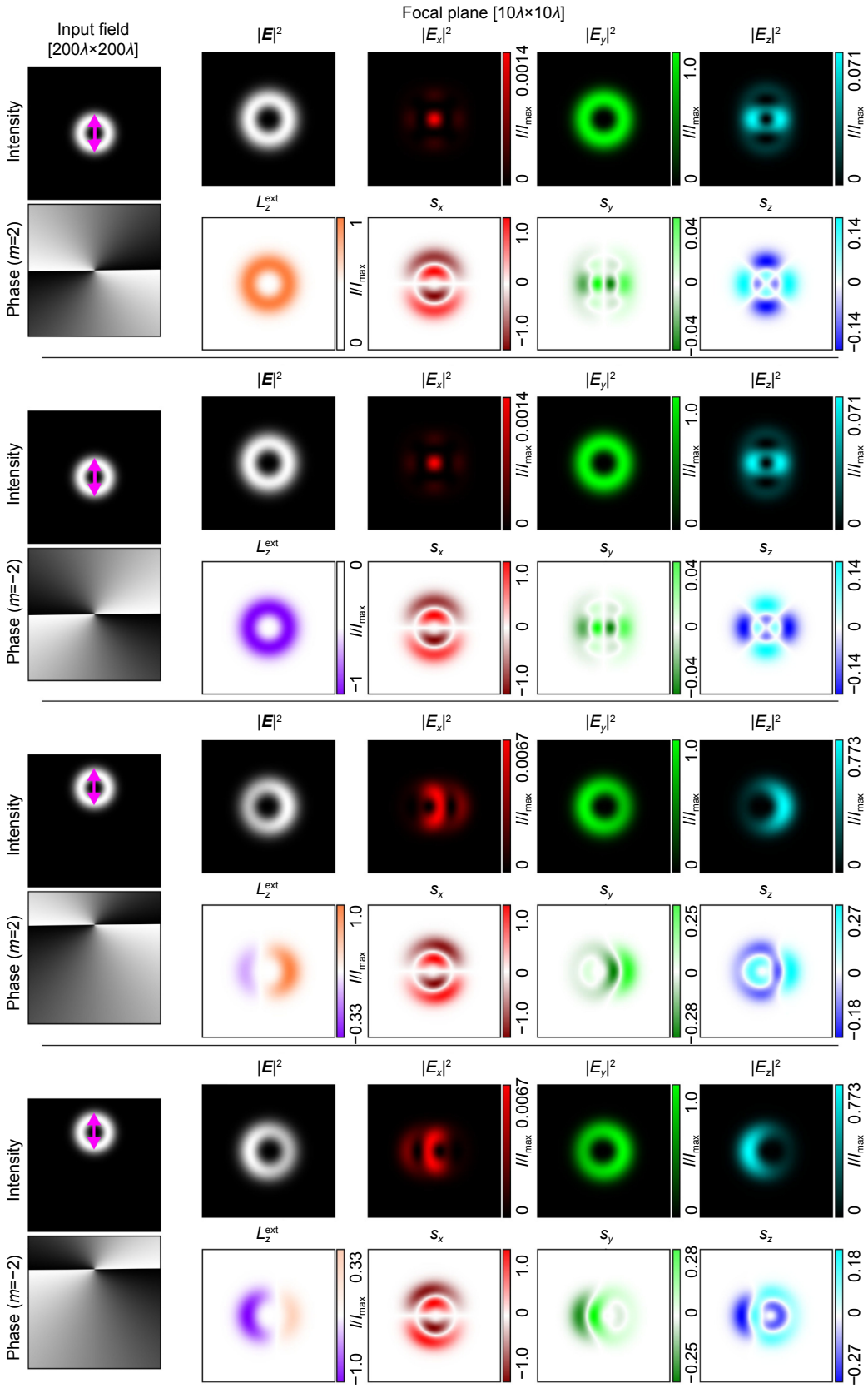

Fig. 5 | Comparison of asymmetry in focusing a shifted vortex beam with *m*=±2 order for *y*-linear polarization.

$$|E_z^{\mathrm{cir}+}(u,v,0)|^2 = I_m(u,v)\left[\left(\frac{2}{w_0^2}(\mathrm{sgn}(m)v^2 - u^2) - k(\mathrm{sgn}(m)\alpha_0 v + \beta_0 u) + (1-\mathrm{sgn}(m))|m|\right)^2 + \left(k(\alpha_0 u - \mathrm{sgn}(m)\beta_0 v) - \frac{2uv}{w_0^2}(1+\mathrm{sgn}(m))\right)^2\right]. \quad (42)$$

In a horizontal section, asymmetry is associated with β_0:

$$\left|E_z^{\mathrm{cir}+}(u,0,0)\right|^2 = I_m(u,0) \cdot \left[\left(-\frac{2u^2}{w_0^2} - k\beta_0 u + (1-\mathrm{sgn}(m))\,|m|\right)^2 + k^2\alpha_0^2 u^2\right], \quad (43)$$

and in the vertical section, the asymmetry is associated with α_0:

$$\left|E_z^{\mathrm{cir}+}(0,v,0)\right|^2 = I_m(0,v) \cdot \left[\left(-\frac{2v^2}{w_0^2} - k\alpha_0 v + (1-\mathrm{sgn}(m))\,|m|\right)^2 + k^2\beta_0^2 u^2\right]. \quad (44)$$

The results for "–" circular polarization will be similar with the corresponding sign change.

Note, Eqs. (43) and (44) become simpler when the direction of polarization and rotation of the vortex coincide, i.e. when $m > 0$ ($\mathrm{sgn}(m) = 1$):

$$\left|E_z^{\mathrm{cir}+}(u,0,0)\right|^2 = I_{m>0}(u,0)\left[\left(-\frac{2u^2}{w_0^2} - k\beta_0 u\right)^2 + k^2\alpha_0^2 u^2\right]. \quad (45)$$

$$\left|E_z^{\mathrm{cir}+}(0,v,0)\right|^2 = I_{m>0}(0,v)\left[\left(\frac{2v^2}{w_0^2} - k\alpha_0 v\right)^2 + k^2\beta_0^2 v^2\right]. \quad (46)$$

The expressions for the transverse components are rather cumbersome and difficult to analyze, however, the results of numerical simulation allow us to draw certain conclusions.

The results of modeling the focusing of a field with "+" and "–"-circular polarization both in the absence of a disturbance and with a vertical shift (α_0= 0, β_0=0.5) are shown in Figs. 6, 7 for various values of m. As can be seen, a more complex spin-orbit interaction occurs.

The main result of the analytical and numerical simulations presented above is that upon focusing of an asymmetric beam possessing angular momentum all three Cartesian components of the electric field in the focal plane experience shifts and/or are redistributed. These changes are required in order to conserve the AM. Most prominently, the longitudinal component of OAM of such a beam, which is an extrinsic one, must be conserved, and it is expressed as $L_z^{\mathrm{ext}} = \sigma(1 - \cos\theta) + m$[8,9]. Here σ is the SAM/helicity, θ is the convergence angle of the ray upon focusing, and m is the topologic charge of the vortex. This equality exhibits the dominance of the OAM/handedness over the SAM/helicity in the Hall effect of light due to both the higher available values of m as compared to σ (which can be 1 or −1) and due to the factor of $(1 - \cos\theta)$. While this expression displays the spin-orbit and orbit-orbit (internal OAM to external OAM) conversion, our results exhibit also orbit-spin conversion/interaction. Namely, the appearance of shifted/asymmetric distributions of s_z and s_y (and to some extent, s_x too) for linearly polarized asymmetric vortex input beam tells that OAM is either directly transformed to SAM and/or acts as a catalyzer to redistribution of SAM, as noticed when focusing a radially polarized vortex beam[25]. We note that while a specific SAM component's center of gravity may not be shifted and its integral over space is unchanged upon focusing, its distribution can be affected by the asymmetric field components. For example, $s_z \sim E_x^* E_y$ and since these field components shift in opposite directions -the center of gravity of s_z (and its magnitude) is practically not affected while its distribution is changed. On the other hand, $s_y \sim E_x^* E_z$ and since both of those components shift in the same direction, the center of gravity of s_y follows the center of gravity of intensity, as noticed also in ref.[9]. In general, the spin redistribution can be accompanied by OAM conversion to spin, and the pattern becomes quite complicated. Evidently, the presence of OAM makes the spin-orbital Hall effect of light more complex and richer than the spin Hall effect. In both cases, one can claim that the electric field components "self-organize" to fulfill the AM conservation law. It should be noted that a recent publication[5] presents a comprehensive study of spin Hall effect of light dependence on the incoming beam off-axis distance, its azimuthal sector masking as well as horizontal masking, and our results are in accordance with this study.

From our simulations, it is seen that except for the case of input x-polarization, when the displaced input beam produced z-component in the focal plane is negligible, in all instances the longitudinal/z-component shift/asymmetry is dominant/the most discernible as

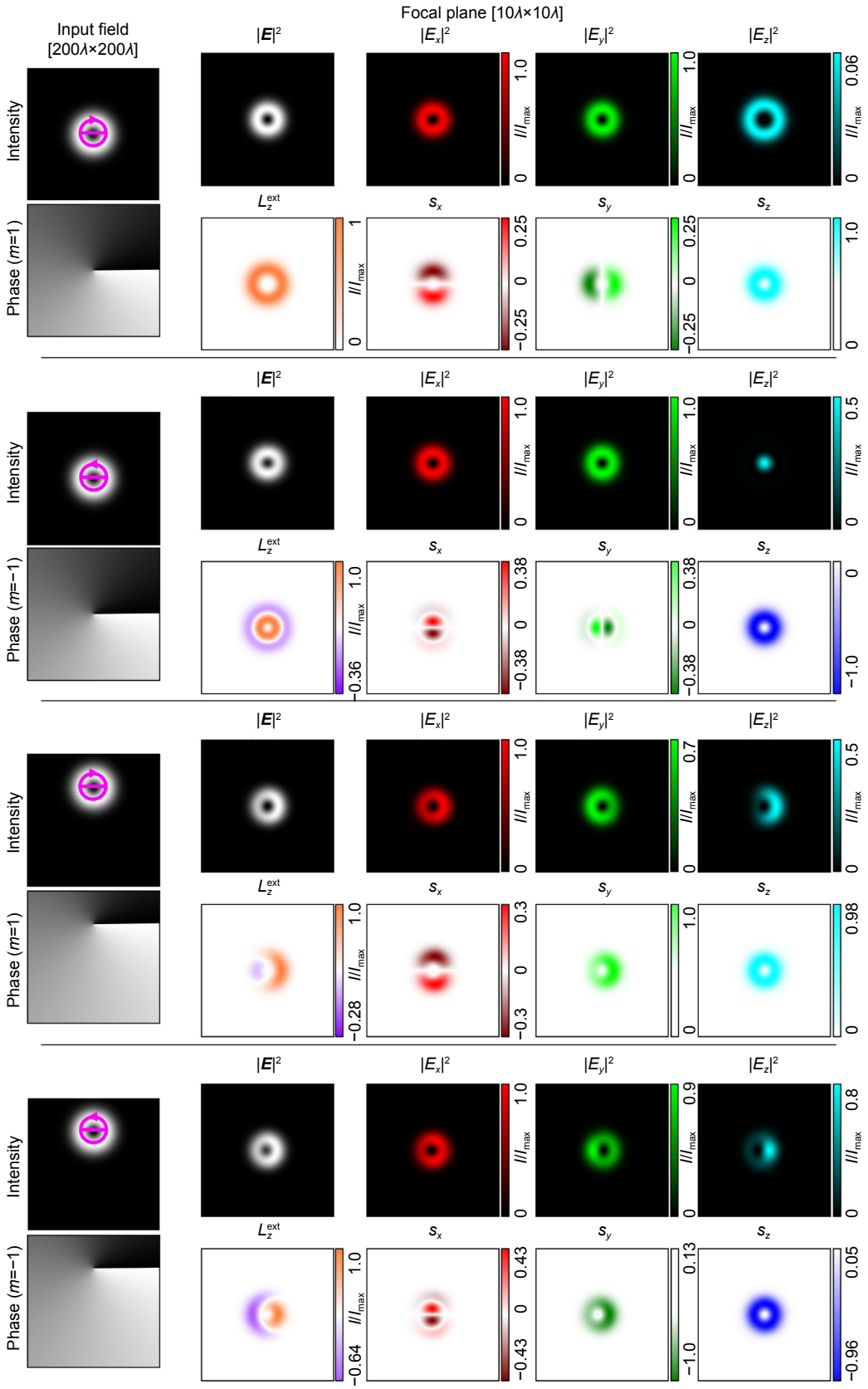

Fig. 6 | Comparison of asymmetry in focusing a shifted vortex beam with *m*=+1 order for "±" -circular polarization.

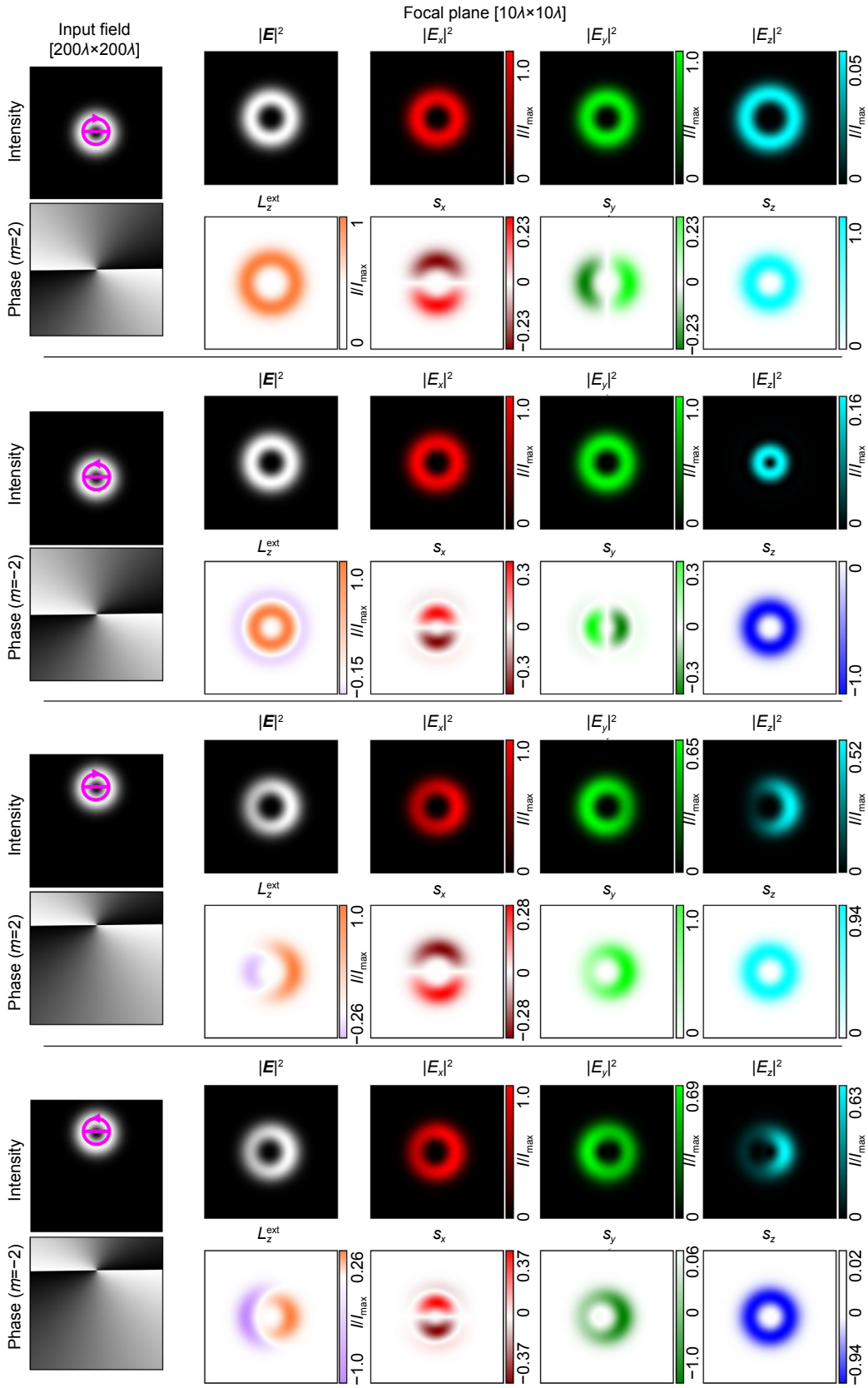

Fig. 7 | Comparison of asymmetry in focusing a shifted vortex beam with *m*=+2 order for "±"-circular polarization.

compared to the displacements/asymmetry of other components or that of the total intensity. This is due to the fact that different transverse components shift in opposite directions and thus their combined contribution to intensity shift/asymmetry is marginal. Consequently, an experiment measuring the distribution of the longitudinal component is performed and discussed in the following section.

Experimental results

For experimental verification of the numerically obtained results, we used laser patterning of thin azopolymer films with the designed structured laser beams. Previously, it was shown that thin azopolymer films, for example, the thin films fabricated from carbazole-based polymer 9-(2,3-epoxypropyl) carbazole (EPC) and azo-dye Disperse Orange 3 (DO3)[26] are polarization sensitive[27–30]. Such materials can be effectively used for visualization of the longitudinal component of the illuminating laser beam[31,32]. In fact, the intensity distribution of the longitudinal component can be used as the expected profile of the nano- and microstructures formed because of laser patterning of a thin azopolymer film. This was repeatedly shown in several studies with laser beams structured in amplitude, phase and/or polarization[33–39]. In the experiments, we used a thin azopolymer film with thickness of 1.5 μm the preparation procedure of which is described in details in ref.[32].

The optical setup is shown in Fig. 8. In these experiments, we used a linearly polarized Gaussian beam from a solid-state laser source (wavelength λ is 532 nm, maximum output laser power P_{out} is 90 mW). The used thin azopolymer film has transmission of about 50% at the wavelength of the laser. The laser beam was collimated and expanded with a combination of lenses L1 and L2 with focal lengths of 25 and 150 mm. For the modulation of the phase distribution of the initial Gaussian laser beam, a reflective spatial light modulator (SLM) HOLOEYE PLUTO VIS (1920×1080 pixels, pixel size of 8 μm) was used. For generation of OV beams with ±1 topological charge, we used a phase mask in the form of a blazed fork-shaped grating (the inset in Fig. 8 shows an example of the used mask). Mirrors M1–M5 were used in the optical setup for steering the laser beam. A combination of two lenses L3 and L4 with focal lengths of 500 and 400 mm, as well as a circular diaphragm D were used for spatial filtering of the modulated laser beam reflected from the SLM. For rotation of the initial linear polarization of the laser beam or its transformation into a right- or left-handed circular polarization, we used a half or a quarter wave plate PE. The modulated laser beam structured in phase and/or polarization was directed into the input pupil of a micro-objective MO1 (*NA* = 0.65). This microobjective was mounted on the 3-axis

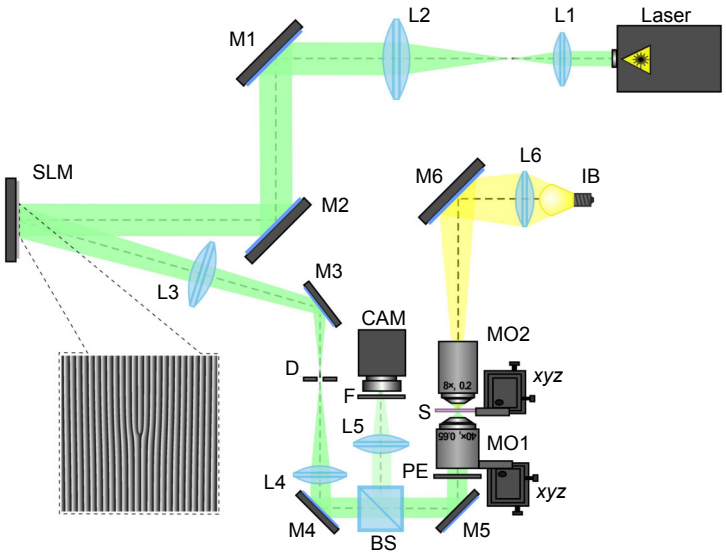

Fig. 8 | The experimental setup for laser printing. Laser is a solid-state laser (λ=532 nm); L1, L2, L3, L4, L5, and L6 are spherical lenses (f_1=25 mm, f_2=150 mm, f_3=500 mm, f_4=400 mm, f_5=150 mm, and f_6=50 mm); M1, M2, M3, M4, M5, and M6 are mirrors, SLM is a reflective spatial light modulator (HOLOEYE PLUTO VIS); D is a circular diaphragm, BS is a beam splitter, PE is a polarizing element (a half wave or a quarter wave plate), MO1 and MO2 are microobjectives (*NA*=0.65 and 0.1); S is a glass substrate with a thin azopolymer film; *xyz* is a three-axis (*XYZ*) translation stage, IB is a light bulb, F is a neutral density filter, CAM is a ToupCam UCMOS08000KPB video camera. The inset shows an example of a phase mask realized with the SLM and used for the generation of a first-order OV beam.

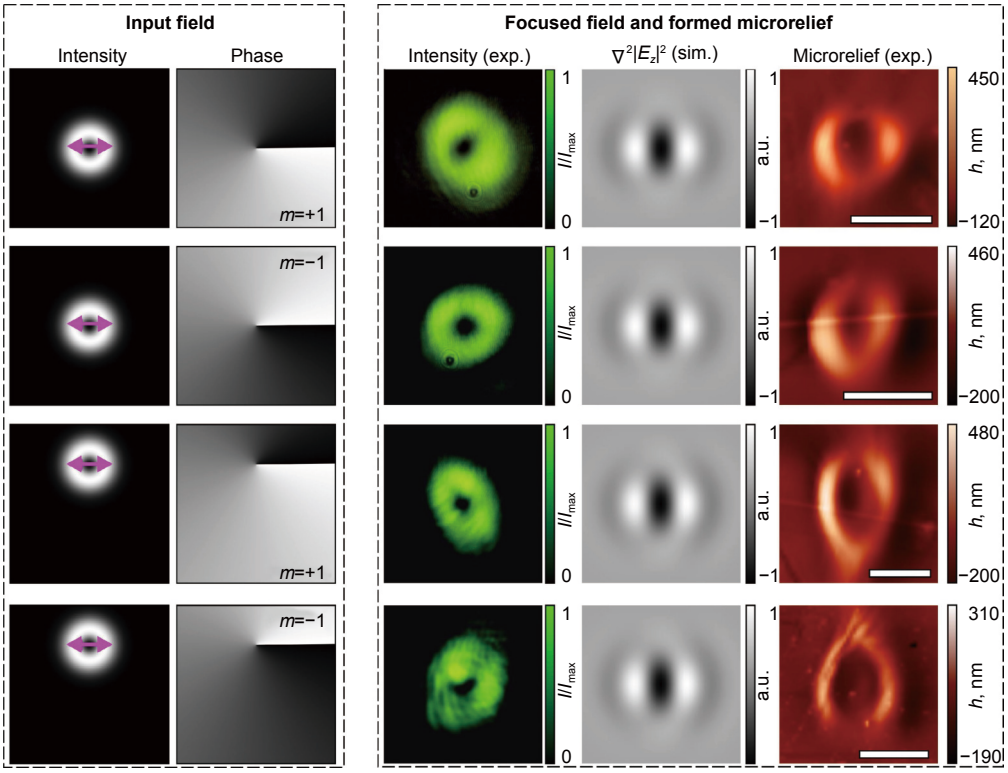

Fig. 9 | Laser patterning of an azopolymer thin film with *x*-linearly polarized on- and off-axis OV beams of ±1 order. The right part of the figure shows the experimentally generated intensity distribution, numerically calculated distribution of $\nabla^2|E_z|^2$, and atomic force microscopy (AFM) images of microreliefs fabricated in the azopolymer thin film. The scale bar is 5 μm.

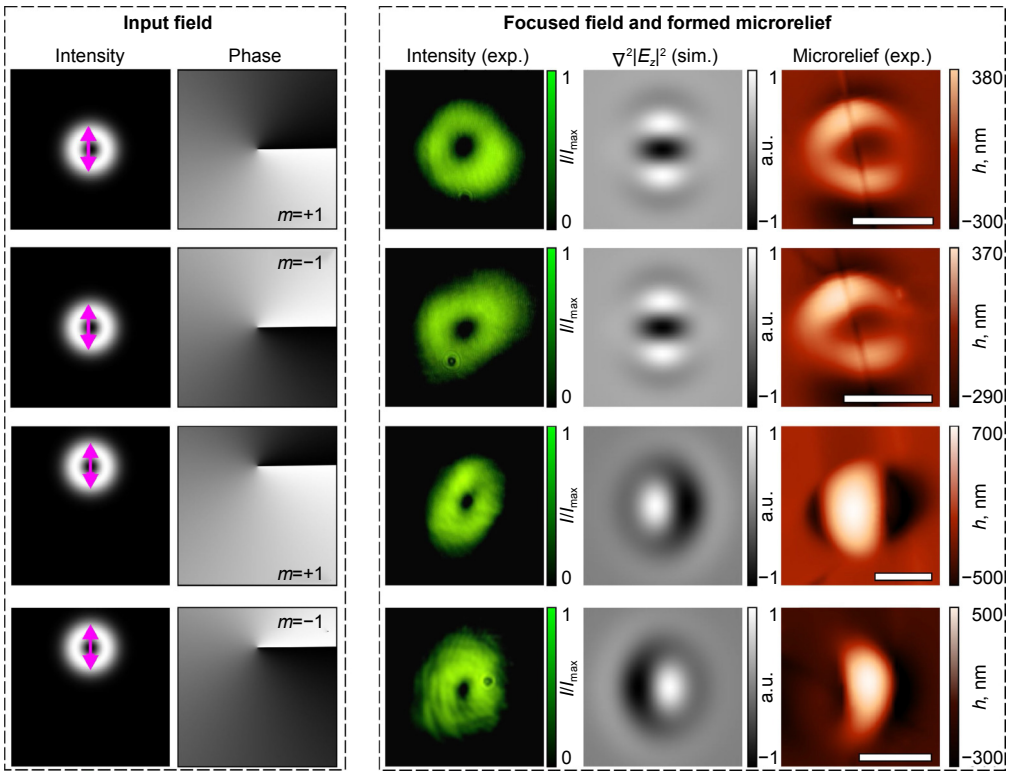

Fig. 10 | Laser patterning of an azopolymer thin film with *y*-linearly polarized on- and off-axis OV beams of ±1 order. The right part of the figure shows the experimentally generated intensity distribution, numerically calculated distribution of $\nabla^2|E_z|^2$, and AFM images of microreliefs fabricated in the azopolymer thin film. The scale bar is 5 μm.

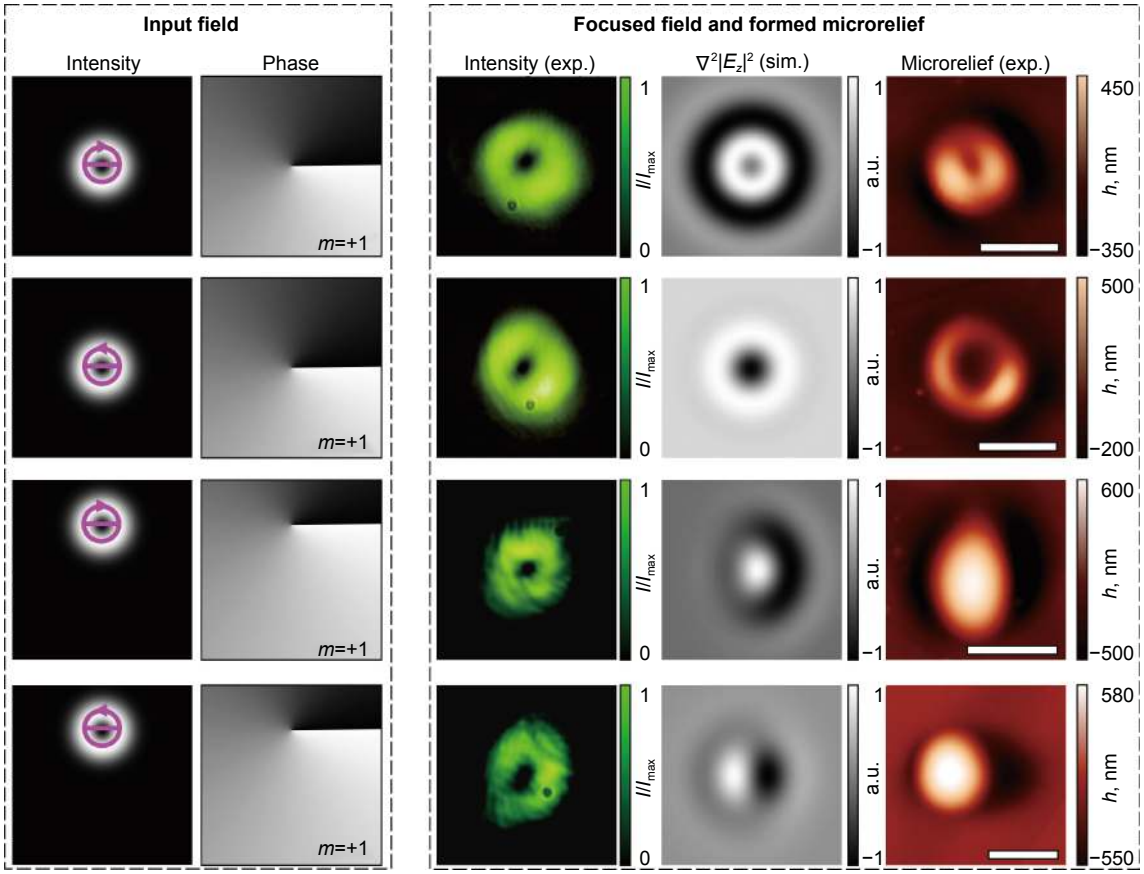

Fig. 11 | Laser patterning of an azopolymer thin film with right- and left handed circularly polarized on- and off-axis OV beams of ±1 order. The right part of the figure shows the experimentally generated intensity distribution, numerically calculated distribution of $\nabla^2|E_z|^2$, and AFM images of microreliefs fabricated in the azopolymer thin film. The scale bar is 5 μm.

XYZ translation stage, which allowed us to move it in the transverse plane and shift it relative to the beam propagation axis. The glass substrate S with a thin azopolymer film was also mounted on the 3-axis *XYZ* translation stage and located in the focal plane of the micro-objective MO1. A system consisting of a light bulb IB, a spherical lens L6 (focal length of 50 mm), a mirror M6, and a micro-objective MO2 (*NA* = 0.1) was used to illuminate the surface of the glass substrate. A system consisting of a beam splitter BS, a lens L5 (focal length of 150 mm), a video camera CAM (TOUPCAM UHCCD00800KPA; 1600 × 1200 pixels, with a pixel size of 3.34 μm), and a neutral density filter F was used to observe the surface of the processed glass substrate during laser processing.

The profiles of the microstructures fabricated under illumination of various structured laser beams (*x*- and *y*-linearly polarized and right- and –left hand circularly polarized OV beams of ±1 order) are shown in Figs. 9–11. These profiles were obtained with a scanning probe microscope NT-MDT SOLVER Pro-M (a semi-contact operating mode, the tip curvature radius of the probe did not exceed 10 nm, the line scanning frequency was 0.5 Hz, the study area is 30×30 μm^2). The profiles of the fabricated microstructures coincides well with the distributions of $\nabla^2|E_z|^2$ which actually corresponds to the inversion of the intensity of the longitudinal component. Previously, these distributions have shown good agreements with the three-dimensional profiles of microreliefs formed in thin azopolymer films when they were illuminated by linearly and circularly polarized vortex beams[33], high-order cylindrical beams and their combinations[32], and interferometrically shaped multi-spiral circularly polarized laser fields[34]. We can conclude that these experimentally obtained results are in good agreement with numerically obtained ones and clearly indicate the vectorial spin-orbital Hall effect of light upon focusing.

Conclusions

We have shown that in spin-orbital Hall effect of light upon tight focusing of an asymmetric beam different

Cartesian components in the focus are shifted perpendicular to the symmetry breaking axis by different amounts and in opposite directions. It is found that in addition to spin-orbit and orbit-orbit, orbit-spin conversions and reorganization takes place. Experiments confirm our analytical and numerical calculations. For experimental studies, just the longitudinal component of the electric field was chosen and the effect of the considered parameters on the formation of an asymmetric relief was demonstrated. In particular, when the direction of displacement coincides with the direction of polarization, the asymmetry is determined by the sign of the optical vortex. For circular polarization, the picture is more complicated, since it is important that the direction of rotation of the polarization and the optical vortex correspond. These findings elucidate the Hall effect of light and may expand the spectrum of its applications.

References

1. Liu L, Chen SS, Lin ZZ, Zhang X. A symmetry-breaking phase in two-dimensional $FeTe_2$ with ferromagnetism above room temperature. *J Phys Chem Lett* **11**, 7893–7900 (2020).
2. Córdova C, Ohmori K, Rudelius T. Generalized symmetry breaking scales and weak gravity conjectures. *J High Energy Phys* **2022**, 154 (2022).
3. Devínsky F. Chirality and the origin of life. *Symmetry* **13**, 2277 (2021).
4. Yang SH, Naaman R, Paltiel Y, Parkin SSP. Chiral spintronics. *Nat Rev Phys* **3**, 328–343 (2021).
5. Cheng JH, Zhang Z, Mei W, Cao Y, Ling XH et al. Symmetry-breaking enabled topological phase transitions in spin-orbit optics. *Opt Express* **31**, 23621–23630 (2023).
6. Baranova NB, Savchenko AY, Zel'dovich BY. Transverse shift of a focal spot due to switching of the sign of circular polarization. *JETP Lett* **59**, 232–234 (1994).
7. Aiello A, Lindlein N, Marquardt C, Leuchs G. Transverse angular momentum and geometric spin hall effect of light. *Phys Rev Lett* **103**, 100401 (2009).
8. Bliokh KY, Alonso MA, Ostrovskaya EA, Aiello A. Angular momenta and spin-orbit interaction of nonparaxial light in free space. *Phys Rev A* **82**, 063825 (2010).
9. Zhu WG, She WL. Transverse angular momentum and transverse barycenter shift of a focused light field due to nonuniform input angular momentum. *Opt Lett* **39**, 1337–1340 (2014).
10. Khonina SN, Golub I. Vectorial spin Hall effect of light upon tight focusing. *Opt Lett* **47**, 2166–2169 (2022).
11. Porfirev A, Khonina S, Kuchmizhak A. Light–matter interaction empowered by orbital angular momentum: control of matter at the micro-and nanoscale. *Prog Quantum Electron* **88**, 100459 (2023).
12. Bliokh KY, Rodríguez-Fortuño FJ, Nori F, Zayats AV. Spin–orbit interactions of light. *Nat Photonics* **9**, 796–808 (2015).
13. Khonina SN, Golub I. Breaking the symmetry to structure light. *Opt Lett* **46**, 2605–2608 (2021).
14. Zhang Z, Mei W, Cheng JH, Tan YW, Dai ZP et al. Revisiting vortex generation in the spin-orbit interactions of refraction and focusing of light. *Phys Rev A* **106**, 063520 (2022).
15. Richards B, Wolf E. Electromagnetic diffraction in optical systems II. Structure of the image field in an aplanatic system. *Proc Roy Soc A:Math Phys Sci* **253**, 358–379 (1959).
16. Pereira SF, van de Nes AS. Superresolution by means of polarisation, phase and amplitude pupil masks. *Opt Commun* **234**, 119–124 (2004).
17. Bokor N, Davidson N. A three dimensional dark focal spot uniformly surrounded by light. *Opt Commun* **279**, 229–234 (2007).
18. Khonina SN, Volotovskiy SG, Fidirko NS. Iterative approach to solve the inverse diffraction problem under sharp focusing conditions. *Opt Mem Neural Netw* **26**, 18–25 (2017).
19. Mansuripur M. Certain computational aspects of vector diffraction problems. *J Opt Soc Am A* **6**, 786–805 (1989).
20. Kogelnik H, Li T. Laser beams and resonators. *Appl Opt* **5**, 1550–1567 (1966).
21. Enderlein J, Pampaloni F. Unified operator approach for deriving Hermite–Gaussian and Laguerre–Gaussian laser modes. *J Opt Soc Am A* **21**, 1553–1558 (2004).
22. Volotovskiy SG, Karpeev SV, Khonina SN. Algorithm for reconstructing complex coefficients of Laguerre–Gaussian modes from the intensity distribution of their coherent superposition. *Comput Opt* **44**, 352–362 (2020).
23. Goodman JW. *Introduction to Fourier Optics* (McGraw-Hill, San Francisco, 1968).
24. Marcuse D. *Light Transmission Optics* 2nd ed (Van Nostrand Reinhold, New York, 1982).
25. Han L, Liu S, Li P, Zhang Y, Cheng HC et al. Catalystlike effect of orbital angular momentum on the conversion of transverse to three-dimensional spin states within tightly focused radially polarized beams. *Phys. Rev. A* **97**, 053802 (2018).
26. Meshalkin A, Losmanschii C, Prisacar A, Achimova E, Abashkin V et al. Carbazole-based azopolymers as media for polarization holographic recording. *Adv Phys Res* **1**, 86–98 (2019).
27. Priimagi A, Shevchenko A. Azopolymer-based micro-and nanopatterning for photonic applications. *J Polym Sci Part B Polym Phys* **52**, 163–182 (2014).
28. Sekkat Z, Wood J, Aust EF, Knoll W, Volksen W et al. Light-induced orientation in a high glass transition temperature polyimide with polar azo dyes in the side chain. *J Opt Soc Am B* **13**, 1713–1724 (1996).
29. Sekkat Z, Kawata S. Laser nanofabrication in photoresists and azopolymers. *Laser Photonics Rev* **8**, 1–26 (2014).
30. Sava I, Hurduc N, Sacarescu L, Apostol I, Damian V. Study of the nanostructuration capacity of some azopolymers with rigid or flexible chains. *High Perform Polym* **25**, 13–24 (2013).
31. Ishitobi H, Nakamura I, Kobayashi TA, Hayazawa N, Sekkat Z et al. Nanomovement of azo polymers induced by longitudinal fields. *ACS Photonics* **1**, 190–197 (2014).
32. Porfirev A, Khonina S, Ivliev N, Meshalkin A, Achimova E et al. Writing and reading with the longitudinal component of light using carbazole-containing azopolymer thin films. *Sci Rep* **12**, 3477 (2022).
33. Porfirev AP, Khonina SN, Khorin PA, Ivliev NA. Polarization-sensitive direct laser patterning of azopolymer thin films with vortex beams. *Opt Lett* **47**, 5080–5083 (2022).
34. Porfirev AP, Ivliev NA, Fomchenkov SA, Khonina SN. Multi-spiral laser patterning of azopolymer thin films for generation of orbital angular momentum light. *Nanomaterials* **13**, 612 (2023).

35. Ambrosio A, Marrucci L, Borbone F, Roviello A, Maddalena P. Light-induced spiral mass transport in azo-polymer films under vortex-beam illumination. *Nat Commun* **3**, 989 (2012).
36. Sekkat Z. Vectorial motion of matter induced by light fueled molecular machines. *OSA Continuum* **1**, 668–681 (2018).
37. Sekkat Z. Model for athermal enhancement of molecular mobility in solid polymers by light. *Phys Rev E* **102**, 032501 (2020).
38. Masuda K, Shinozaki R, Kinezuka Y, Lee J, Ohno S et al. Nanoscale chiral surface relief of azo-polymers with nearfield OAM light. *Opt Express* **26**, 22197–22207 (2018).
39. Masuda K, Shinozaki R, Shiraishi A, Ichijo M, Yamane K et al. Picosecond optical vortex-induced chiral surface relief in an azo-polymer film. *J Nanophoton* **14**, 016012 (2020).

Acknowledgements

The work was supported by the Russian Science Foundation grant No. 22-79-10007.

Author contributions

S Khonina and I Golub proposed the original idea and supervised the project. A Ustinov and S Khonina carried out theoretical analysis. S Khonina performed numerical modelling. A Porfirev performed the experiments. N Ivliev performed the measurements of the profiles of the fabricated microstructures.

Competing interests

The authors declare no competing financial interests.